FORMULATION AND IMPLEMENTATION OF A CONSTITUTIVE MODEL FOR BRITTLE MATERIALS IN ABAQUS EXPLICIT FINITE ELEMENT CODE

Daniel Bürger, bur.daniel@gmail.com
Instituto de Aeronáutica e Espaço - IAE

Maurício Vicente Donadon, donadon@ita.br
Instituto Tecnológico de Aeronáutica - ITA

Francisco Cristóvão Lourenço de Melo, frapi@iae.cta.br
Instituto de Aeronáutica e Espaço - IAE

Sérgio Frascino Müller de Almeida, frascino@ita.br
Instituto Tecnológico de Aeronáutica - ITA

Abstract.*This paper presents in details the formulation of the Johnson-Holmquist constitutive model (JH-2) for brittle materials. The model formulation is presented within the updated Lagrangian formulation context using a stress update algorithm fully compatible with the central difference time integration scheme commonly used in explicit finite element code for brick elements. Details on the model implementation and validation are also presented and discussed. Finally, an aplication of this model is shown by simulating the impact of a projectile onto a mixed ceramic-composite armour.*

Keywords: *brittle materials, constitutive model, finite elements, ballistic impact, armour*

1. INTRODUCTION

Nowadays, armours are made with two or more materials in order to improve the structural performance, with less weight, more mobility and ensuring the same protection. As the prices of the materials involved in the experiments increase, the need for developing accurate simulation tools becomes more important. New high performance armour is composed of a ceramic plate, to avoid the armour-piercing (AP) projectiles, and a composite base, usually made with aramid, or more recently, ultra high molecular weight polyethylene (UHMWPE), that absorbs the projectile energy and hold fragments of the projectile and the ceramic. This work presents a numerical model for ballistic impact simulations in hybrid ceramic/fiber reinforced composite armours. The simulations were carried out using ABAQUS/Explicit finite element code. Four different material models have been used for this purpose: (i) Johnson-Cook model to predict the material behavior of the projectile, (ii) JH-2 model to predict the material behavior of the ceramic, (iii) a 3-D progressive failure model to predict the structural response of the composite base, (iv) a contact-logic to predict debonding between the ceramic plate and the composite base. The material models (ii), (iii) and (iv) have been implemented into ABAQUS as user defined material models within solid elements. Details on the models are given in section 2. The aim of the model is to achieve an accurate V_{50}, that is, the velocity at which there is a 50% probability of specimen penetration in the armour. Different models were ran at different initial velocities, and then the results were evaluated to find out if the armour supports the impact or the projectile defeats the armour.

2. CONSTITUTIVE MODELS

2.1 JH-2 model

2.1.1 Description of the JH-2 model

The JH-2 model is a constitutive model suitable to predict the behavior of brittle materials subjected to extreme loading. The main features of the model includes pressure-dependent strength, damage and fracture, significant strength after fracture, bulking and strain rate effects. A general overview of the JH-2 model in terms of strength is shown in Fig. 1. The idea behind the model formulation is that the material begins to soften when damage begins to accumulate ($D > 0$). This allows for gradual softening of the material under increasing plastic strain. The strength and pressure are normalized by the strength and pressure components of the Hugoniot Elastic Limit (HEL), which allows for many constants to be dimensionless. The strength and damage are analytic functions of the pressure and other variables allowing for parametric variation of the constants in a systematic manner. The strength generally is a smoothly varying function of the intact strength, fracture strength, strain rate and damage (Johnson and Holmquist, 1994).

The normalized equivalent stress shown in Fig. 1 is defined in Eq. (1), where σ_i^* is the normalized intact equivalent stress, σ_f^* is the normalized fracture strength stress and D is the damage ($0 \leq D \leq 1$) (Johnson and Holmquist, 1994). The normalized equivalent stresses (σ^*, σ_i^*, σ_f^*) have the general form given in Eq. (2), where σ is the actual equivalent stress and σ_{HEL} is the equivalent stress at the HEL defined in Eq. (3).

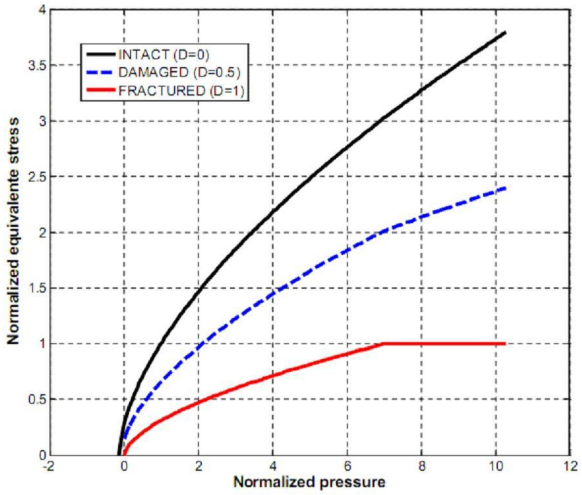

Figure 1. Description of the JH-2 model

$$\sigma^* = \sigma_i^* - D(\sigma_i^* - \sigma_f^*) \tag{1}$$

$$\sigma^* = \frac{\sigma}{\sigma_{HEL}} \tag{2}$$

$$\sigma_{HEL} = \frac{3}{2}(HEL - P_{HEL}) \tag{3}$$

The HEL is the net axial stress for the Hugoniot Elastic Limit and P_{HEL} is the pressure component of the HEL. The normalized intact strength is given by Eq. (4), and the normalized fracture strength is given by Eq. (5), where the normalized fracture strength can be limited by $\sigma_f^* \leq \sigma_{fmax}^*$ with $\sigma_{fmax}^* = 1$ that is, $\sigma_f = \sigma_{HEL}$.

$$\sigma_i^* = A(P^* + T^*)^N(1 + Cln(\dot{\varepsilon}^*)) \tag{4}$$

$$\sigma_f^* = B(P^*)^M(1 + Cln(\dot{\varepsilon}^*)) \tag{5}$$

The material constants are A, B, C, M, N and σ_{fmax}. The normalized pressure is defined as $P^* = P/P_{HEL}$ where P is the actual pressure and P_{HEL} is the pressure at HEL. The normalized maximum tensile hydrostatic stress is $T^* = T/P_{HEL}$, where T is the maximum tensile hydrostatic pressure the material can withstand. The dimensionless strain rate is $\dot{\varepsilon}^* = \dot{\varepsilon}/\dot{\varepsilon}_0$, where $\dot{\varepsilon}$ is the actual strain rate and $\dot{\varepsilon}_0$ is the reference strain rate. The damage for fracture is accumulated in a manner similar to that used in Johnson-Cook fracture model (Johnson and Cook, 1985), and it is expressed in Eq. (6). $\Delta\varepsilon_p$ is the equivalent plastic strain increment during a cycle of integration and $\varepsilon_f^p = f(P)$ is the plastic strain to fracture under constant pressure. The expression for ε_f^p is given in Eq. (7), where D_1 and D_2 are material constants. The plastic strain rate vector for a three dimensional stress state can be obtained from the Prandtl-Reuss flow rules given in Eq. (8) (Crisfield, 2003).

$$D = \sum \frac{\Delta\varepsilon_p}{\varepsilon_f^p} \tag{6}$$

$$\varepsilon_f^p = D_1(P^* + T^*)^{D_2} \tag{7}$$

$$\begin{Bmatrix} \dot{\varepsilon}_{xx}^p \\ \dot{\varepsilon}_{yy}^p \\ \dot{\varepsilon}_{zz}^p \\ \dot{\varepsilon}_{xy}^p \\ \dot{\varepsilon}_{yz}^p \\ \dot{\varepsilon}_{zx}^p \end{Bmatrix} = \dot{\lambda} \begin{Bmatrix} \partial F(\bar{\sigma}, \sigma_{HEL}, \sigma^*)/\partial S_{xx} \\ \partial F(\bar{\sigma}, \sigma_{HEL}, \sigma^*)/\partial S_{yy} \\ \partial F(\bar{\sigma}, \sigma_{HEL}, \sigma^*)/\partial S_{zz} \\ \partial F(\bar{\sigma}, \sigma_{HEL}, \sigma^*)/\partial S_{xy} \\ \partial F(\bar{\sigma}, \sigma_{HEL}, \sigma^*)/\partial S_{yz} \\ \partial F(\bar{\sigma}, \sigma_{HEL}, \sigma^*)/\partial S_{zx} \end{Bmatrix} = \dot{\lambda} a \tag{8}$$

Where $\dot{\lambda}$ is the plastic strain rate multiplier and $F(\bar{\sigma})$ is the yield function given by Eq. (9). $\bar{\sigma}$ is the equivalent stress which is defined in terms of the deviatoric stresses as presented in Eq. (10).

$$F(\bar{\sigma}) = \bar{\sigma} - \sigma_{HEL}.\sigma^* \tag{9}$$

$$\bar{\sigma} = \sqrt{3}\Big[\frac{1}{2}(S_{xx}^2 + S_{yy}^2 + S_{zz}^2) + S_{xy}^2 + S_{yz}^2 + S_{zx}^2\Big]^{\frac{1}{2}} \tag{10}$$

Substituting Eq. (10) into Eq. (9) the Eq. (8) can be rewritten as presented in Eq. (11). The equivalent plastic strain is given by Sun (2002), and presented in Eq. (12). Substituting Eq. (11) into Eq. (12) we obtain Eq. (13). For plastic flow to occur, the stresses must remain on the yield surface and hence we have Eq. (14).

$$\begin{Bmatrix} \dot{\varepsilon}_{xx}^p \\ \dot{\varepsilon}_{yy}^p \\ \dot{\varepsilon}_{zz}^p \\ \dot{\varepsilon}_{xy}^p \\ \dot{\varepsilon}_{yz}^p \\ \dot{\varepsilon}_{zx}^p \end{Bmatrix} = \frac{3\dot{\lambda}}{2\bar{\sigma}} \begin{Bmatrix} S_{xx} \\ S_{yy} \\ S_{zz} \\ S_{xy} \\ S_{yz} \\ S_{zx} \end{Bmatrix} \tag{11}$$

$$\dot{\varepsilon_p} = \sqrt{\frac{2}{9}\Big[(\dot{\varepsilon}_{xx}^p - \dot{\varepsilon}_{yy}^p)^2 + (\dot{\varepsilon}_{xx}^p - \dot{\varepsilon}_{zz}^p)^2 + (\dot{\varepsilon}_{yy}^p - \dot{\varepsilon}_{zz}^p)^2 + \frac{3}{2}\Big[(\dot{\varepsilon}_{xy}^p)^2 + (\dot{\varepsilon}_{yz}^p)^2 + (\dot{\varepsilon}_{zx}^p)^2\Big]\Big]} \tag{12}$$

$$\dot{\varepsilon_p} = \frac{\dot{\lambda}}{\sqrt{2}}\sqrt{(S_{xx} - S_{yy})^2 + (S_{xx} - S_{zz})^2 + (S_{yy} - S_{zz})^2 + 6\Big[S_{xy}^2 + S_{yz}^2 + S_{zx}^2\Big]} \tag{13}$$

$$F(\bar{\sigma}, \sigma_{HEL}, \sigma^*) = \frac{\partial F}{\partial \sigma}\dot{\sigma} = a^T\dot{\sigma} \tag{14}$$

The situation described by Eq. (14) implies that during the plastic flow the stress changes $\dot{\sigma}$ are instantaneously moving tangentially to the surface with $\dot{\sigma}$ being orthogonal to the vector a. Hence in the present formulation a is normal to the surface and the flow rules invoke normality. By decomposing the total strain rate into elastic and plastic strain rate components the stress-strain rates relationship showed in Eq. (15) can be obtained. Where C is the material stiffness matrix which has been assumed to be macroscopically isotropic. Substituting Eq. (15) into Eq. (14) we obtain the expression for $\dot{\lambda}$ presented in Eq. (16). Substituting Eq. (16) into Eq. (13) results in Eq. (17).

$$\dot{\sigma} = C(\dot{\varepsilon} - \dot{\varepsilon}_p) = C(\dot{\varepsilon} - \dot{\lambda}a) \tag{15}$$

$$\dot{\lambda} = \frac{a^T C\dot{\varepsilon}}{a^T Ca} \tag{16}$$

$$\Delta\varepsilon_p = \frac{a^T C\dot{\varepsilon}\Delta T}{\sqrt{2}a^T Ca}\sqrt{(S_{xx} - S_{yy})^2 + (S_{xx} - S_{zz})^2 + (S_{yy} - S_{zz})^2 + 6\Big[S_{xy}^2 + S_{yz}^2 + S_{zx}^2\Big]} \tag{17}$$

The hydrostatic stresses are defined in terms of the pressure given by the following equation of state (EOS), Eq. (18). $K_1 = E/(3(1-2\nu))$ is the bulk modulus, K_2 and K_3 are material constants. μ is the compressibility factor which is given by Eq. (19). Where $\varepsilon_\nu = \varepsilon_{xx} + \varepsilon_{yy} + \varepsilon_{zz}$ is the volumetric strain. For tensile pressure ($\mu < 0$), $P = K_1\mu$. After damage begins to accumulate ($D > 0$), bulking can occur. Now an additional incremental pressure, ΔP is added, such in Eq. (20).

$$P = K_1\mu + K_2\mu^2 + k_3\mu^3 \tag{18}$$

$$\mu = \frac{\rho}{\rho_0} - 1 = -ln(\varepsilon_\nu) \tag{19}$$

$$P = K_1\mu + K_2\mu^2 + k_3\mu^3 + \Delta P \tag{20}$$

The pressure increment is determined from energy considerations: it varies from $\Delta P = 0$ at $D = 0$ to $\Delta P = \Delta P_{max}$ at $D = 1$. The incremental internal elastic energy decrease due to decreased shear and deviator stress is converted to potential internal energy by incrementally increasing ΔP. The decrease in the shear and deviator stress occurs because the strength decreases as damage increases (see Fig. 1). The expression for the elastic internal energy of shear and deviatoric stress is showed in Eq. (21) (Johnson and Holmquist, 1994). Where G is the shear modulus of elasticity. The incremental energy loss is defined in Eq. (22) (Johnson and Holmquist, 1994). Where U_D^t and $U_D^{t+\Delta t}$ are computed from Eq. (21) using the updated stresses at the current step $\sigma^{t+\Delta t}$ for both energies. Johnson and Holmquist (1994) shown that

if the energy loss ΔU is converted to potential hydrostatic energy through ΔP the Eq. (23), for the pressure increment can be obtained. Where β is the fraction of the elastic energy loss converted to potential hydrostatic energy.

$$U = \frac{(\sigma_{HEL}.\sigma^*)^2}{6G} \tag{21}$$

$$\Delta U = U_D^t - U_D^{t+\Delta t} \tag{22}$$

$$\Delta P^{t+\Delta t} = -K_1\mu^{t+\Delta t} + \sqrt{(-K_1\mu^{t+\Delta t} + \Delta P^t) + 2\beta K_1 \Delta U} \tag{23}$$

2.1.2 Numerical implementation

The JH-2 model has been implemented into ABAQUS Explicit finite element code within brick elements. The code formulation is based on the updated Lagrangian formulation which is used in conjunction with the central difference time integration scheme for integrating the resultant set of nonlinear dynamic equations. The method assumes a linear interpolation for velocities between two subsequent time steps and no stiffness matrix inversions are required during the analysis. The drawback of the explicit method is that it is conditionally stable for nonlinear dynamic problems and the stability for its explicit operator is based on a critical value of the smallest time increment for a dilatational wave to cross any element in the mesh. Details on the model implementation are given below in Tab 1.:

Table 1: Details on the model implementation.

Step	Description	Equation
1	Strain update at current time step	$\varepsilon_{ij}^{t+\Delta t} = \varepsilon_{ij}^t + \Delta\varepsilon_{ij}$
2	Compute strain rates	$\dot{\varepsilon}_{ij}^{t+\Delta t} = \Delta\varepsilon_{ij}/\Delta t$
3	Compute strain increments	$\Delta\sigma_{ij} = C\Delta\varepsilon_{ij}$
4	Computa trial stresses at current time step	${}^{trial}\sigma_{ij}^{t+\Delta t} = \sigma_{ij}^t + \Delta\sigma_{ij}$
5	Split total trial stresses into deviatoric and hydrostactic stresses	
5.1	Hydrostatic stress	$\sigma_H^{t+\Delta t} = \frac{1}{3}({}^{trial}\sigma_{11}^{t+\Delta t} + {}^{trial}\sigma_{22}^{t+\Delta t} + {}^{trial}\sigma_{33}^{t+\Delta t})$
5.2	Deviatoric stresses	$S_{ij}^{trial} = {}^{trial}\sigma_{ij}^{t+\Delta t} - \sigma_H^{t+\Delta t}\delta_{ij}$ (1)
6	Compute total effective strain rate	$\dot{\varepsilon} = \sqrt{\frac{2}{3}}\sqrt{\dot{\varepsilon}_{xx}^2 + \dot{\varepsilon}_{yy}^2 + \dot{\varepsilon}_{zz}^2 + \frac{1}{2}(\gamma_{xy}^2 + \gamma_{yz}^2 + \gamma_{zx}^2)}$
7	Compute equivalent $\bar{\sigma}$ stress using Eq. (10)	Eq. (10)
8	Compute normalized yield stress	Eq. (4), (5), (1)
9	Check for yielding	Eq.(9)
9.1	If $F(\bar{\sigma}) > 0$ return the deviatoric stresses to the yield surface using the radial return algorithm	$S_{ij} = (\sigma_{HEL}.\sigma^*)/S_{ij}^{trial}$
9.2	Compute the plastic strain increment $\Delta\varepsilon_p$ using Eq. (17)	Eq. (17)
9.3	Compute the plastic strain to fracture ε_f^p using Eq. (7)	Eq. (7)
9.4	Update the damage variable D	$D^{t+\Delta t} = D^t + (\Delta\varepsilon_p)/\varepsilon_f^p$
10	Compute the compressibility factor	$\mu^{t+\Delta t} = ln(\varepsilon_\nu^{t+\Delta t} + 1)$
10.1	If $\mu^{t+\Delta t} > 0$ compute pressure from equation of state Eq. (20)	Eq.(20)
10.2	Else if $\mu^{t+\Delta t} < 0$,	$P^{t+\Delta t} = K_1\mu^{t+\Delta t}$
10.3	If $D^{t+\Delta t} > 0$ compute energy loss due to damage using Eqs. (21) and (22) with	$U_D^t = (\sigma_i^* - D^t(\sigma_i^* - \sigma_f^*).\sigma_{HEL})^2/(6G)$ $U_D^{t+\Delta t} = (\sigma_i^* - D^{t+\Delta t}(\sigma_i^* - \sigma_f^*).\sigma_{HEL})^2/(6G)$
10.4	And compute the pressure increment $\Delta P^{t+\Delta t}$ using Eq. (23)	$P^{t+\Delta t} = \sigma_H^{t+\Delta t} + \Delta P^{t+\Delta t}$
11	Compute new total stress	$\sigma_{ij}^{t+\Delta t} = S_{ij} + P^{t+\Delta t}\delta_{ij}$
12	Go to step 1	

(1) $\delta_{ij} = 1$ for $i = j$ and $\delta_{ij} = 0$ otherwise

2.1.3 Validation

Johnson and Holmquist (1994) present three validation cases for this constitutive model. All cases involve the confined compression and release of a ceramic material with variation of damage representation to demonstrate the response of the model. For all three cases the model consists of a cube with sides 1.0 meter in length modeled using a single three-dimensional element. The displacements on five faces of the element were constrained in respect to the faces normal direction, and loaded under normal displacement control on the sixth face (top). For each test, the material was displaced vertically downwards by 0.05 m and then released until a zero stress-state was reached. Due to bulking, the final volume of the material was larger than the original volume resulting in a non-zero displacement corresponding to zero stress. Table 2 present the material properties for the three validation cases.

Table 2. Material model constants.

	Case A	Case B	Case C	Unity
Density	3700	3700	3700	Kg/m^3
Shear modulus	9.016 10^{10}	9.016 10^{10}	9.016 10^{10}	Pa
Strength constants				
A	0.93	0.93	0.93	
B	0	0	0.31	
C	0	0	0	
M	0	0	0.6	
N	0.6	0.6	0.6	
Ref. strain rate	1.0	1.0	1.0	
T	2 10^8	2 10^8	2 10^8	Pa
HEL	2.79 10^9	2.79 10^9	2.79 10^9	Pa
P_{HEL}	1.46 10^9	1.46 10^9	1.46 10^9	Pa
D_1	0.0	0.005	0.005	
D_2	0.0	1.0	1.0	
K_1	1.3095 10^{11}	1.3095 10^{11}	1.3095 10^{11}	Pa
K_2	0.0	0.0	0.0	Pa
K_3	0.0	0.0	0.0	Pa
β	1.0	1.0	1.0	

For case A, the material was defined as having no fractured strength and was not allowed to accumulate plastic strain. As such, the material is fully damaged once the strength was exceeded. This led to an instantaneous increase in bulking pressure of 0.56 GPa. In case B, the material was defined as having no fractured strength but was allowed to accumulate plastic strain so that complete damage did not occur instantaneously. In this case the bulking pressure increased with damage to a maximum value of 0.72 GPa when the material was completely damaged. Case C incorporated both fractured material strength and the accumulation of plastic strain. A comparison between predictions obtained using the actual JH-2 implemented into ABAQUS and the results published by Johnson and Holmquist (1994) for cases A, B and C is depicted in Fig. 2.

2.2 Johnson-Cook model

The Johnson-Cook model (1983) is a phenomenological model that is commonly used to predict the material response of metals subjected to impact and penetration, since it can reproduce strain hardening, strain-rate effects and thermal softening. These properties are coupled in a multiplicative manner, as shown in Eq. (24), where ε^p_{eff} is the effective plastic strain, T_M is the melting temperature, T_R is the reference temperature when determining C_1, C_2 and C_4, $\dot{\varepsilon}_0$ is the reference strain rate; C_1, C_2, C_3, C_4 and C_5 are material constants. The fracture in the Johnson-Cook model (1985) is based on the value of the equivalent plastic strain. Failure is assumed to occur when damage exceeds 1. The cumulative-damage fracture model is presented in Eq. (25) and (26), where P is the pressure, $\sigma_{eff}$is the Mises stress; D_1, D_2, D_3, D_4, D_5 are failure parameters.

$$\sigma_y = \left[C_1 + C_2(\varepsilon^p_{eff})^{C_4}\right]\left(1 + C_3 ln\left(\frac{\dot{\varepsilon}^p_{eff}}{\dot{\varepsilon}_0}\right)\right)\left[1 - \left(\frac{T - T_R}{T_M - T_R}\right)^{C_5}\right] \tag{24}$$

$$D = \sum \frac{\Delta\varepsilon^p_{eff}}{\varepsilon^F} \tag{25}$$

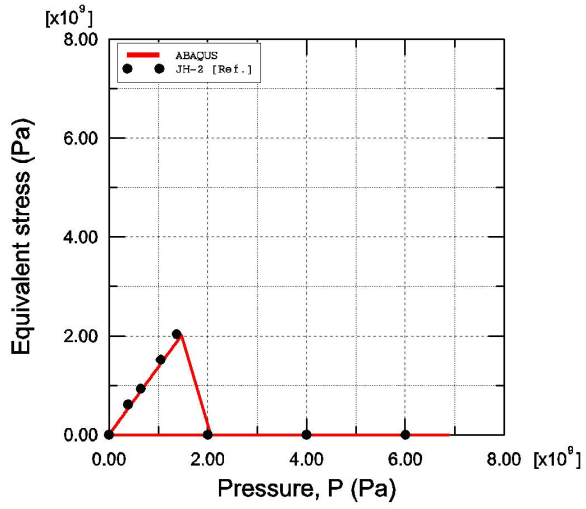

(a) Case A

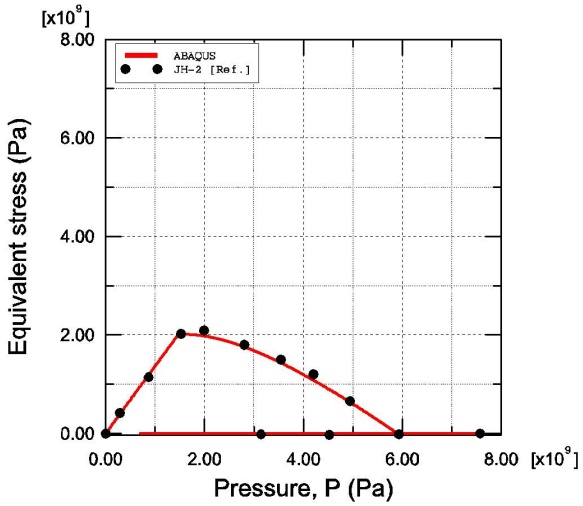

(b) Case B

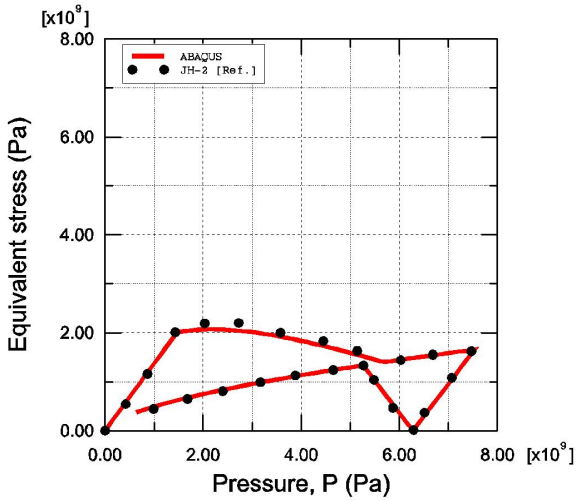

(c) Case C

Figure 2. Stress versus pressure histories for single element validation

$$\varepsilon^F = \left[D_1 + D_2 exp\left(D_3 \frac{P}{\sigma^{eff}}\right)\right]\left(1 + D_4 ln\left(\frac{\dot{\varepsilon}^p_{eff}}{\dot{\varepsilon}_0}\right)\right)\left[1 + D_5\left(\frac{T - T_R}{T_M - T_R}\right)^{C_5}\right] \tag{26}$$

2.3 Composite failure model

The formulation for this model is based on the Continuum Damage Mechanics (CDM) approach and enables the control of the energy dissipation associated with each failure mode regardless of mesh refinement and fracture plane orientation by using a smeared cracking formulation. Internal thermodynamically irreversible damage variables were defined in order to quantify damage concentration associated with each possible failure mode and predict the gradual stiffness reduction during the fracture process. The material model has been implemented into ABAQUS explicit finite element code within brick elements as a user-defined material model. The criteria used to detect the different damage modes are listed in Tab. 3. Details on the model formulation can be found in Donadon et al. (2009a). Figure 3 shows an example, of normalized stress/damage parameter vs strain for a single element, subjected to a loading-unloading-reloading case. It is clear from Fig. 3 the drop in the stress with increasing damage.

2.4 Contact-logic

The interfacial material behavior is defined in terms of tractions and relative displacements between the upper and lower surfaces defining the interface. The relative displacement vector is composed of the resultant normal and sliding

Table 3. Failure modes and criteria.

Failure mode	Criterion
Fiber failure in tension	$\sigma_1 \geq X_T$
Fiber failure in compression	$\lvert\sigma_1\rvert \geq X_C$
Inter-fiber failure (IFF)	$\left(\frac{\sigma_2}{Y_T}\right)^2 + \left(\frac{\tau_{23}}{S_{23}}\right)^2 + \left(\frac{\tau_{12}}{S_{12}}\right)^2 \geq 1$
In-plane shear failure	$\lvert\tau_{12}\rvert \geq S_{12}$

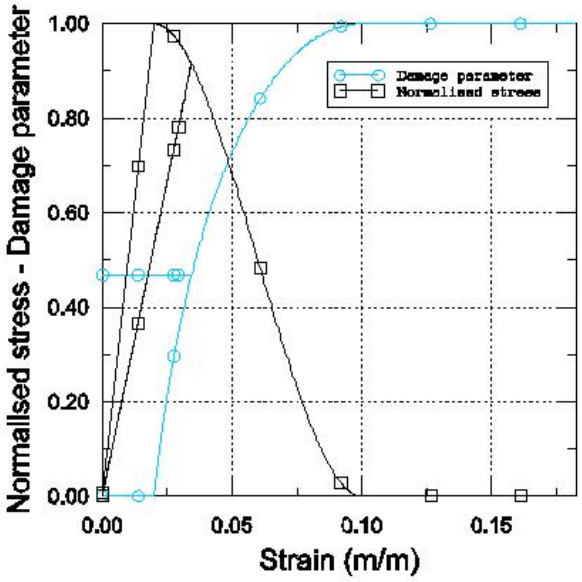

Figure 3. Element loaded-unloaded-reloaded

components defining by the relative movement between upper and lower surfaces of the contact element(see Fig. 4 (a)). The criteria for damage initiation and damage progression are respectively given by Eq. (27) and (28). The constitutive law for a three dimensional stress case is shown in Fig. 4 (c). G_i is the strain energy released rate defined by Eq. (29). K_{ii} is the interfacial stiffness in the direction ii, for $i = I, II, III$, and d is the damage parameter defined in Eq. (30). The mixed-mode delamination damage onset displacement vector is given in Eq. (31), and the final resultant displacement associated with the fully debonded interfacial behavior, is given in Eq. (32), α, and β are defined in Fig. 4 (b), and they are the angles that define the orientation of the relative displacement vector. Details about the formulation are given in Donadon, et al (2009b).

$$\left(\frac{\sigma_I}{\sigma_I^0}\right)^2 + \left(\frac{\sigma_{II}}{\sigma_{II}^0}\right)^2 + \left(\frac{\sigma_{III}}{\sigma_{III}^0}\right)^2 = 1 \tag{27}$$

$$\left(\frac{G_I}{G_{Ic}}\right)^\lambda + \left(\frac{G_{II}}{G_{IIc}}\right)^\lambda + \left(\frac{G_{III}}{G_{IIIc}}\right)^\lambda = 1 \tag{28}$$

$$G_i = \int_0^{\delta_i^f} \sigma_i d\delta_i \rightarrow \sigma_i = K_{ii}(1-d)\delta_i \tag{29}$$

$$d = 1 - \frac{\bar{\delta}_0}{\bar{\delta}}\left[1 + \left(\frac{\bar{\delta} - \bar{\delta}_0}{\bar{\delta}_f - \bar{\delta}_0}\right)^2 . \left(2\left(\frac{\bar{\delta} - \bar{\delta}_0}{\bar{\delta}_f - \bar{\delta}_0}\right) - 3\right)\right] \text{ with } \bar{\delta} = \sqrt{u^2 + v^2 + w^2} \tag{30}$$

$$\bar{\delta}_0 = \left[\left(\frac{K_{ww}cos(\beta)}{\sigma_I^0}\right)^2 + \left(\frac{K_{uu}sin(\beta)cos(\alpha)}{\sigma_{II}^0}\right)^2 + \left(\frac{K_{vv}sin(\beta)sin(\alpha)}{\sigma_{III}^0}\right)^2\right]^{-\frac{1}{2}} \tag{31}$$

$$\bar{\delta}_f = \frac{2}{\bar{\delta}_0}\left[\left(\frac{K_{ww}cos(\beta)}{G_{Ic}}\right)^\lambda + \left(\frac{K_{uu}sin(\beta)cos(\alpha)}{G_{IIc}}\right)^\lambda + \left(\frac{K_{vv}sin(\beta)sin(\alpha)}{G_{IIIc}}\right)^\lambda\right]^{-\frac{1}{\lambda}} \tag{32}$$

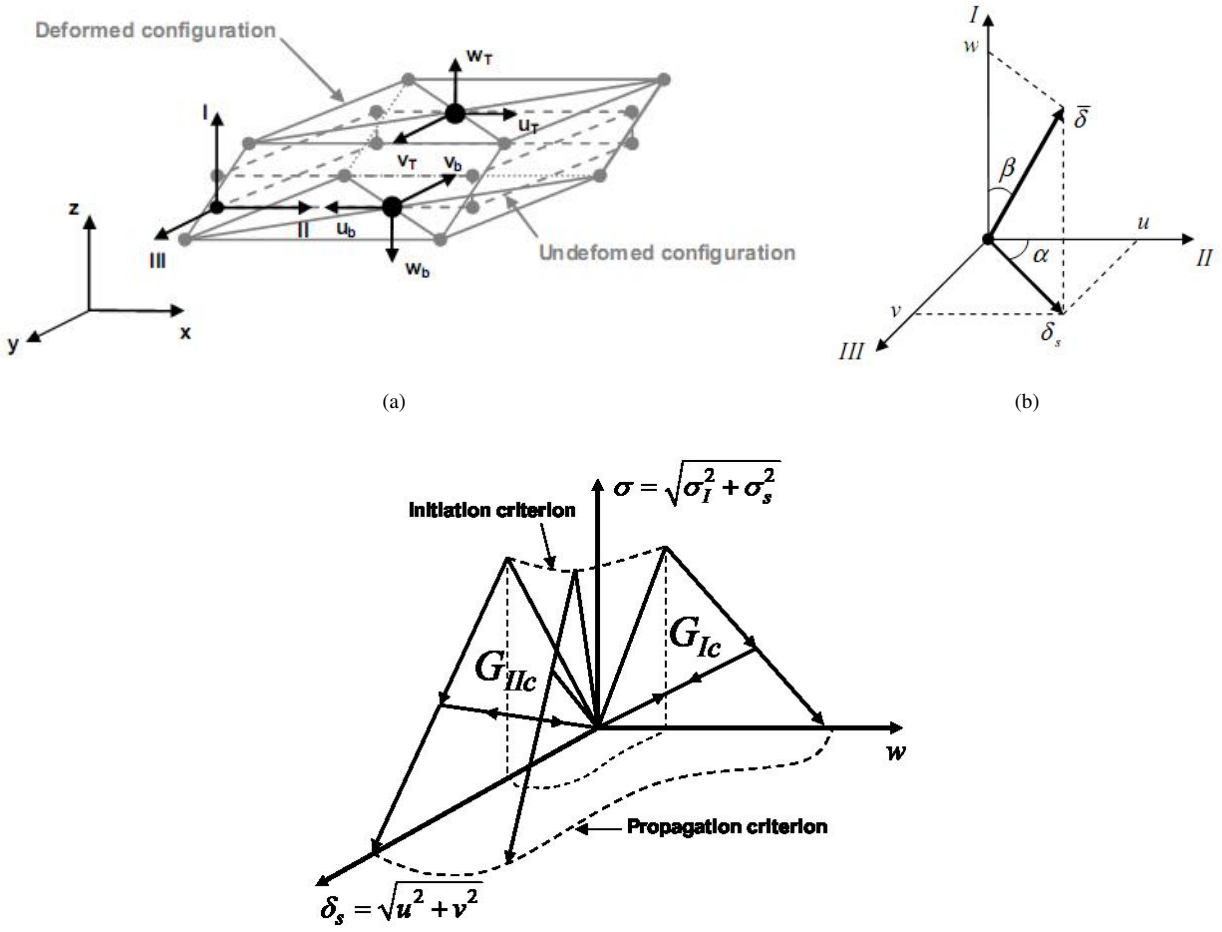

Figure 4. Contact-logic

3. BALLISTIC IMPACT SIMULATIONS

As an application example, these models were used to simulate a ballistic impact. The model consists of a composite base of 0.1 x 0.1 x 0.01 m, with a central hexagonal ceramic plate of thickness 0.1m on the top. The projectile is 7.62 x 51 mm NATO AP made of cooper with a hard steel core. The projectile impacts at the center of the ceramic plate in the normal to the plate direction. The finite element is shown in Fig.5. In this example, to save computational time, it was simulate a quarter of the model only. For boundary conditions it were used: symmetry to divide the model and encastre on the side faces of the composite base. The elements used were: C3D8R, a hexahedral element for the regular model parts and C3D4, a tetrahedron element for the projectile's tip. The contact used was *contact inclusion* with nodal erosion available in ABAQUS finite element code. The constants used in the model are presented in Tabs. 4 and 5. Figure 6 presents the results obtained from the simulations. The figure presents the energy absorbed by armour at impact, and the projectile initial velocity. The simulated V_{50} is around $790m/s$ as indicated in Fig.6.

Table 4: Composite failure model and Johnson-Cook constants used in the model.

Composite model		Johnson-Cook		
Variable	Value	Variable	Cooper	Hard steel
E_1	2.5 10^{10} Pa	C_1	44 10^7 Pa	4.9 10^8 Pa
E_2	2.5 10^{10} Pa	C_2	1.5 10^8 Pa	8.07 10^8 Pa
E_3	3.6 10^9 Pa	C_4	0.31	0.73
ν_{12}	0.046	C_5	1.09	0.94
ν_{13}	0.046	T_M	1083 ^{o}C	1800 ^{o}C
ν_{23}	0.046	T_R	25 ^{o}C	25 ^{o}C
G_{12}	1.08 10^9Pa	C_3	0.025 Pa	0.012 Pa

G_{13}	1.73 10^9Pa	$\dot{\varepsilon}_0$	1	5.0 10^{-4}
G_{23}	1.73 10^9Pa	D_1	0.3	0.0705
X_T	5.4 10^8Pa	D_2	0.28	1.732
G_{1T}	1 $10^5 J/m^3$	D_3	-3.03	-0.54
X_C	6.43 10^7Pa	D_4	0.014	-0.0123
G_{1C}	3 $10^4 J/m^3$	D_5	1.12	0
Y_C	6.43 10^7Pa			
S_{12}	7.7 10^7 Pa			
G_{2C}	3 $10^4 J/m^3$			
S_{23}	5.43 10^8 Pa			

Table 5: JH-2 and contact-logic constants used in the model.

JH-2		Contact-logic	
Variable	Value	Variable	Value
Elasticity modulus	4.4 10^{11} Pa	Element Thickness	1.3 10^{-5}m
Poison coefficient	0.16	E_{33}	1 10^9
Hugoiont Elastic Limit	1.45 10^{10} Pa	G_{13}	1 10^9
Pressure at HEL	5.9 10^9 Pa	G_{23}	1 10^9
A	0.96	N	6 10^7
B	0.75	S_{13}	1 10^8
C	0	S_{23}	1 10^8
N	0.65	G_{Ic}	600
M	1	G_{IIc}	2000
D_1	0.07	G_{IIIc}	2000
D_2	0.48		
S_{fmax}	1		
T	3.7 10^8 Pa		
K_2	0		
K_3	0		
β	1		

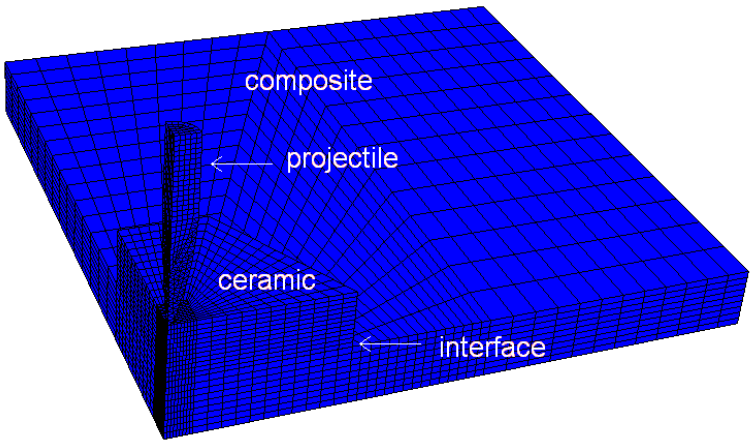

Figure 5. Configuration on the ballistic impact

Figures 7 and 8 present the evolution of projectile penetrating the target. In this figure is presented the results for the case in which $V_{projectile} = 900m/s$. It can be seen in Fig. 7 (d), (e) and (f) the cooper jacket failing. Figure 8 (b) shows the interface initiating failure, and Fig. 8 (f) shows the ceramic completely unstuck from the composite, indicating that the interface has completely failed. The simulations reproduce exactly what happens experimentally when such adhesive (epoxy) is used to bond the ceramic plate into the composite base. Figures 7 (b), (c) and (d) shows the ceramic plate absorbing the initial impact and starting the fragmentation of the projectile. Figure 8 (j) shows the projectile significantly smaller than its initial size, indicating that besides the velocity loss, there was also a mass loss, what is experimentally

proved. Analyzing the simulations it can be concluded that the set of models applied can predict accurately the energy absorption modes and the failure mechanisms involved in armour penetration.

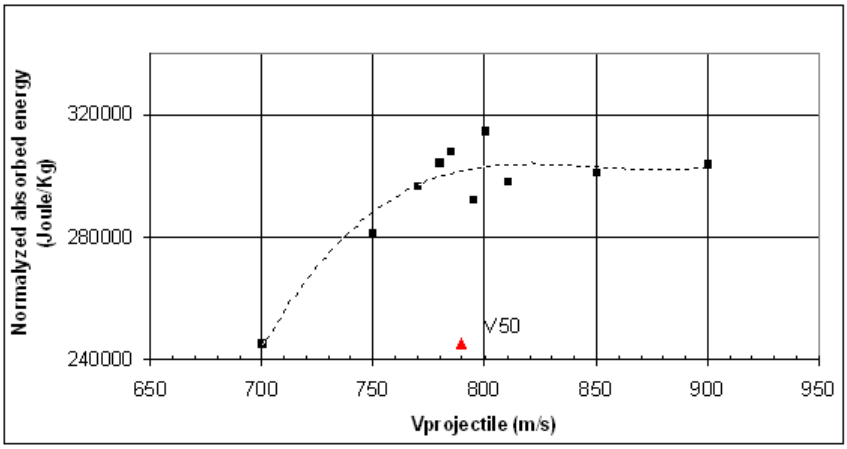

Figure 6. $V_{projectile}$ vs normalized absorbed energy

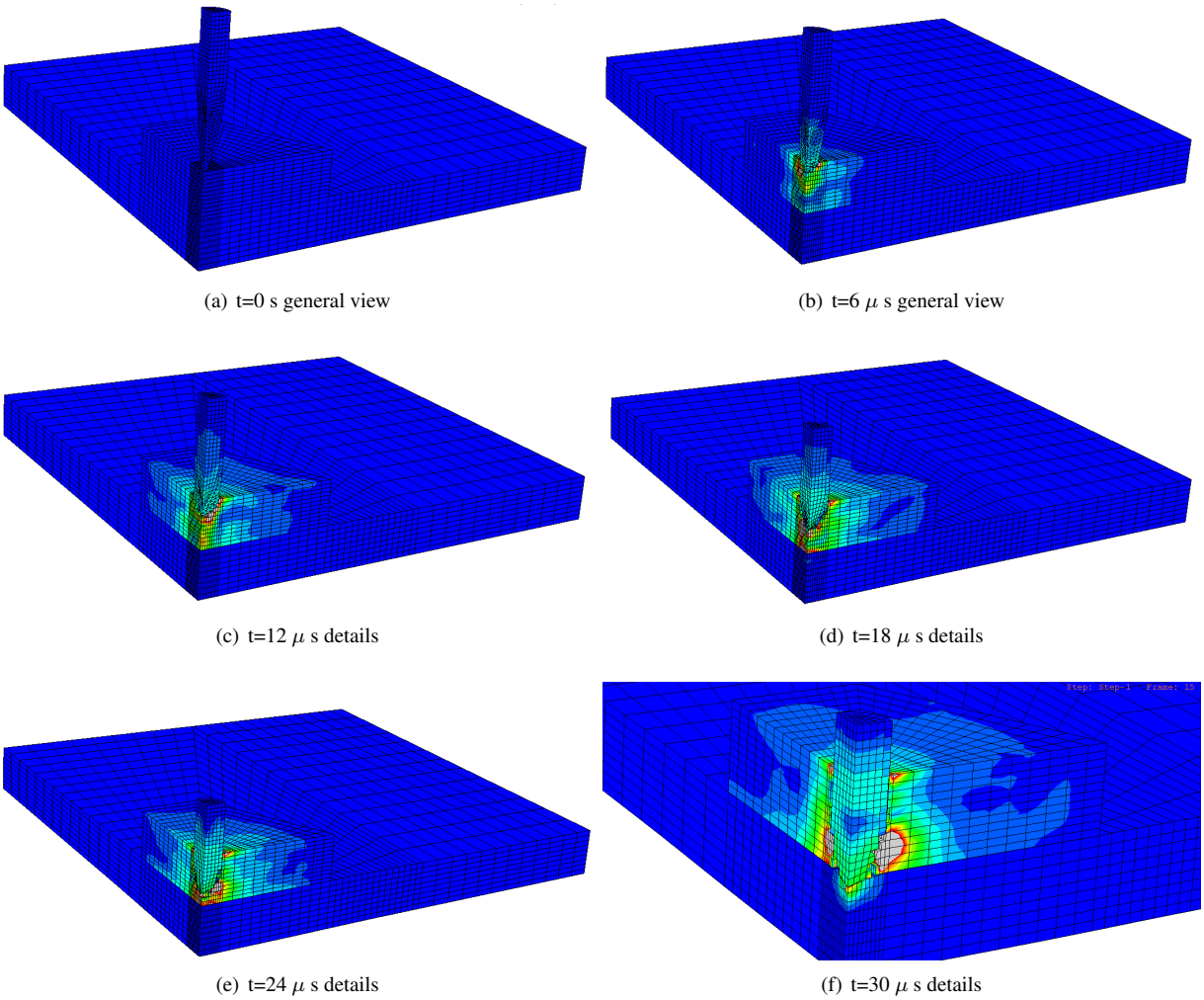

(a) t=0 s general view

(b) t=6 μ s general view

(c) t=12 μ s details

(d) t=18 μ s details

(e) t=24 μ s details

(f) t=30 μ s details

Figure 7. Penetration evolution

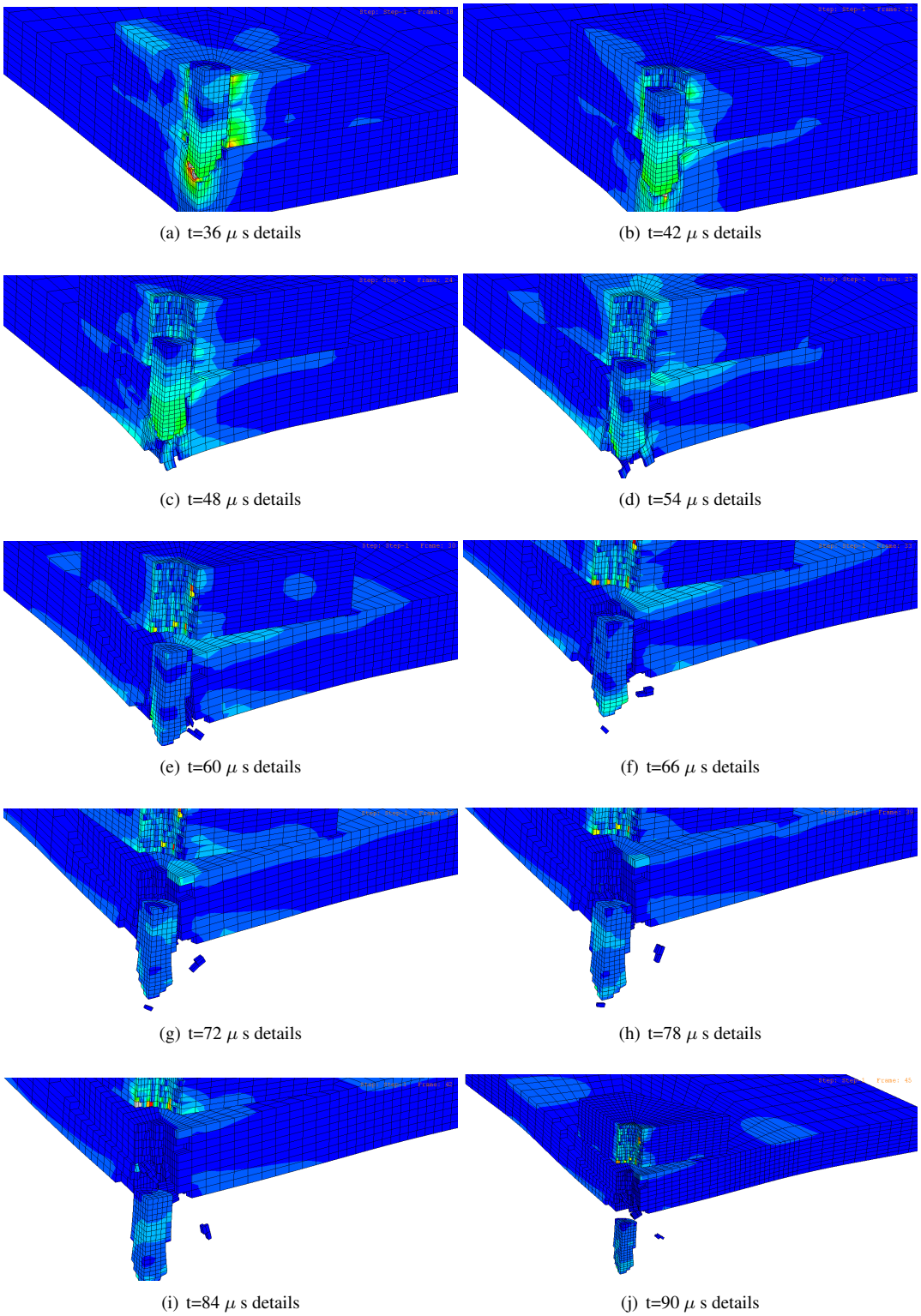

(a) t=36 μ s details (b) t=42 μ s details

(c) t=48 μ s details (d) t=54 μ s details

(e) t=60 μ s details (f) t=66 μ s details

(g) t=72 μ s details (h) t=78 μ s details

(i) t=84 μ s details (j) t=90 μ s details

Figure 8. Penetration evolution

4. ACKNOWLEDGEMENTS

The authors acknowledge the financial support received for this work from Fundação de Amparo à Pesquisa do Estado de São Paulo (FAPESP), contract number 2006/06808-6, and from Financiadora de Estudos e Projetos (FINEP), contract number 2412/06.

5. REFERENCES

Crisfield M.A., 2003, "Non-linear finite element analysis of solids and structures Vol. 1" Ed. John Wiley and Sons.

Donadon M.V., Almeida S.F.M., Arbelo M.A., Faria A.R., 2009a, "A three-dimensional ply failure model for composite structures", International Journal of Aerospace Engineering.

Donadon M.V., Almeida S.F.M., Faria A.R., 2009b, "A contact logic for mixed mode delamination modelling in composite laminates" to be published in an International Journal.

Johnson G.R. and Cook W.H., 1983, "A constitutive model and data for metals subjected to large strains, high strain rate and high temperature", Proceedings of the 7th International Symposium on Ballistics.

Johnson G.R. and Cook W.H., 1985, "Fracture characteristics of three metals subjected to various strain, strain rates, temperatures and pressures", Journal of Engineering Fracture Mechanics, Vol.21, pp 31-48.

Johnson G.R. and Holmquist T.J., 1994, "An improved computational constitutive model for brittle materials", American Institute of Physics, Vol.12, pp. 981-984.

Sun C.T., 2002, "Proceedings of the American Society for Composites" 17th Technical Conference.

6. Responsibility notice

The authors are the only responsible for the printed material included in this paper.